I&EC research
Industrial & Engineering Chemistry Research

Article

Cite This: Ind. Eng. Chem. Res. 2019, 58, 12080−12096

pubs.acs.org/IECR

Optimal Design of Double Pipe Heat Exchanger Structures

Alice Peccini,[†] Julia C. Lemos,[‡] André L. H. Costa,*[,‡] and Miguel J. Bagajewicz[+]

[†]Federal University of Rio de Janeiro (UFRJ), Escola de Química CT, Bloco E, Ilha do Fundão, Rio de Janeiro, Rio de Janeiro CEP 21949-900, Brazil

[‡]Rio de Janeiro State University (UERJ), Rua São Francisco Xavier, 524, Maracanã, Rio de Janeiro, Rio de Janeiro CEP 20550-900, Brazil

[+]School of Chemical, Biological and Materials Engineering, University of Oklahoma, Norman, Oklahoma 73019, United States

Supporting Information

ABSTRACT: This paper investigates the design optimization of double pipe heat exchanger using mathematical programming. The heat exchanger area is minimized and the thermo-fluid dynamic conditions are considered for the use of the right transport correlations, together with design specifications, such as, maximum pressure drops and minimum excess area. The modular nature of this kind of heat exchanger and the allocation of the streams (inside the inner tube or in the annulus) are also contemplated. Two mixed-integer nonlinear programming (MINLP) approaches are proposed. One approach relates the binary variables to the nonlinear constraints directly. In the second, the resulting nonlinearities involving binary variables are formally linearized, without loss of rigor (e.g., no use of truncated Taylor series). The proposed methodology can get better solutions than traditional trial and error procedures. The flexibility of the model is illustrated, together with a comparison between the performances of both MINLP formulations. Additionally, computational time and local optimality issues are discussed.

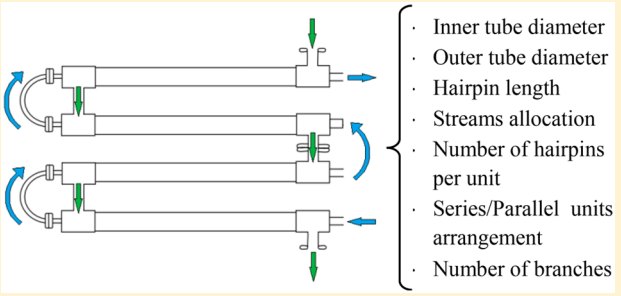

1. INTRODUCTION

Although shell-and-tube heat exchangers are the most common heat transfer equipment in chemical process plants,[1] there are many cases for which other heat exchanger types become more suitable. For instance, double pipe heat exchangers can be an economically more advantageous option when smaller services are in place[2] (e.g., heat transfer area lower than 50 m^2). If the stream contains solids in suspension, double pipe heat exchangers may also be a better alternative, because they can be built with an inner tube with larger diameter to avoid plugging. Smaller diameters of the outer tube in double pipe heat exchangers are advantageous for high-pressure services, because it implies a smaller wall thickness. In addition, double pipe heat exchangers are easily cleaned, and the longitudinal flow avoids the existence of stagnation regions, which in shell and tube exchangers are prone to fouling.[3] Double pipe heat exchangers have also the benefit of flexibility due to its modular structure, which allows an easier adaptation to process modifications.

Several papers addressed the design of double pipe heat exchangers; however, a large number of them are focused on heat transfer enhancement devices, rather than on the general optimization of the equipment design (e.g., diameter and length of the tubes were usually considered fixed parameters).[4] For example, Sahiti et al.[5] investigated the optimization of pin fins in the heat exchanger annulus aiming at the minimization of entropy generation. Their heat exchanger model was based on experimental data and the optimal set of variables was determined through a sensitivity analysis study. In turn, Syed et al.[6] investigated the optimal configuration of the annulus with trapezoidal fins through the selection of the number of fins, fin height, fin thickness, and the radius ratio of the inner and outer tubes, using genetic algorithms and a trust region method. A similar investigation was also proposed by the same authors using parabolic fins[7] and using a generalized optimization of the fin shape.[8] Later, Han et al.[9] investigated the design of the outer surface corrugation of the inner tube using multiobjective optimization for the determination of optimal values of the pitch, height, and radius of the corrugation. Their optimization was based on a response surface methodology (RSM) using simulation data generated through computational fluid dynamics (CFD). Finally, Dastmalchi et al.[10] employed a particle swarm algorithm (PSO) associated with a CFD model for the optimization of the inner microfinned tube surface, contemplating the selection of the number of microfins, the microfin height, and the microfin helix angle.

The aforementioned studies did not account for the operational and capital costs in their objective functions and were focused on enhancing the heat transfer variables such as Nusselt number and heat transfer coefficient, sometimes the

Received: March 21, 2019
Revised: May 16, 2019
Accepted: May 22, 2019
Published: May 22, 2019

DOI: 10.1021/acs.iecr.9b01536
Ind. Eng. Chem. Res. 2019, 58, 12080−12096

minimization of entropy generation, but never discussing a complete optimal design.

Reducing costs is, after all, the main motivation for basic design optimization in practice. The literature involving the solution of the least-cost design problem of double pipe heat exchangers is scarce and the available papers were based on limited search spaces of the geometric variables. First, Söylemez[11] investigated the optimization of double pipe heat exchangers for waste heat recovery, aiming at identifying the inner tube diameter, with a fixed ratio of the diameters of the outer and inner tubes, minimizing capital and operating costs. Later, Swamee et al.[12] presented the optimization of double pipe heat exchangers focusing on operational costs, considering the heat load, the pumping power, and the utility consumption. The decision variables were the inner and outer tube diameters and the utility flow rate, but the tube length was assumed known. In addition, both studies considered the design variables as continuous variables, assuming implicitly that they may lead to suboptimal solutions when the nearest commercially available pipe is selected.

Finally, academic books[2,13] usually use a larger set of design variables (geometric dimensions, fluid allocation, and arrangements with multiple units), and they use a traditional trial and verification procedure; in such procedure, design variables are selected first, followed by the calculation of the number of required hairpins for that configuration. Then, if the resulting heat exchanger is not feasible (e.g., the available pressure drop for a given stream is exceeded and/or the stream velocities are not within given bounds) a design change is proposed and the calculations remade. This work points out that this approach is dependent on the designer experience and does not guarantee any optimality. The designer choices for new trials are various: one can change length, pipe diameters, hairpin arrangements, and other features aiming at reducing pressure drop and/or increasing heat transfer coefficient, and the experts develop the right intuitive choices to end up with a feasible exchanger, which is the goal. It is for this reason that it is rare to see a set of rules as what adjustment in geometry leads to the right answer. In addition, it is unusual to see a trial−verification−improvement procedure in which changes are proposed to seek improvements over the feasible solutions found. In other words, in trial and verification, optimality is definitely not the goal, and even in trial−verification−improvement, optimality is not guaranteed.

To ameliorate the aforementioned deficiencies in the quest for the optimal design, this paper presents the economic optimization of the design of double pipe heat exchangers using a mathematical programming method that at the very least guarantees local optimality. The models are based on the hairpin as the elementary component, arranged in series to form what is here defined as a unit. These units are then considered as the basic component of arrangements in series, parallel, and series-parallel, and thus the modular structure of double pipe heat exchangers is explored.

In addition, the set of design variables considered in this study is broader than the one used in previous literature papers, considering the allocation of the streams (inside the inner tube or in the annulus), the inner and outer tube diameters, the tube length, the number of parallel branches, the number of units in series and in parallel in each branch, and the number of hairpins per unit, which determine the arrangement of the existent hairpins. The optimization problem is formulated as a mixed-integer nonlinear programming (MINLP) model. The fact that several geometric parameters (diameters, lengths, etc.) can be expressed in a form of discrete choices, as in industrial practice, is used as a convenient tool. A modified MINLP model, for which mathematical transformations are applied to exclude nonlinearities involving binary variables is also presented, so that methods requiring linearity in binary variables (like Outer Approximation[14]) can solve the model.

This paper is organized as follows: Initially the model is presented, followed by the first corresponding MINLP formulation and the modified MINLP problem formulation. To finish, numerical results are presented.

2. HEAT EXCHANGER ARCHITECTURE

The basic structure of a double pipe heat exchanger consists of two concentric tubes (Figure 1) and is usually commercialized in

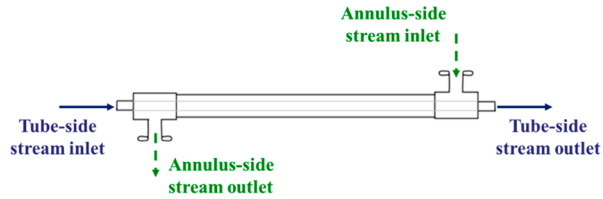

Figure 1. Double pipe heat exchanger.

a hairpin structure (Figure 2). If the thermal service demands a higher heat transfer area, several hairpins can be interconnected. For example, Figure 3 illustrates two hairpins connected in series.

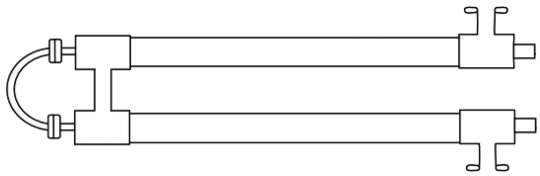

Figure 2. Hairpin structure.

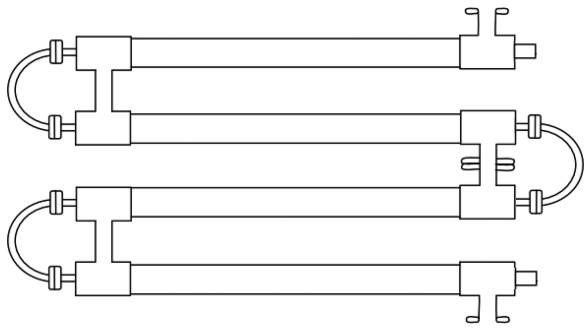

Figure 3. Two hairpins connected in series.

Different interconnection patterns among the heat exchanger hairpins provide flexible design alternatives better suited to attain the heat load and maximum pressure drop specifications of the service. The mathematical formulation proposed explores a general structure that encloses different arrangements. For that, the adopted nomenclature for the elements involved is as follows:

- hairpin: basic structure shown in Figure 2. The flow arrangement for a hairpin in this paper is always countercurrent

DOI: 10.1021/acs.iecr.9b01536
Ind. Eng. Chem. Res. 2019, 58, 12080−12096

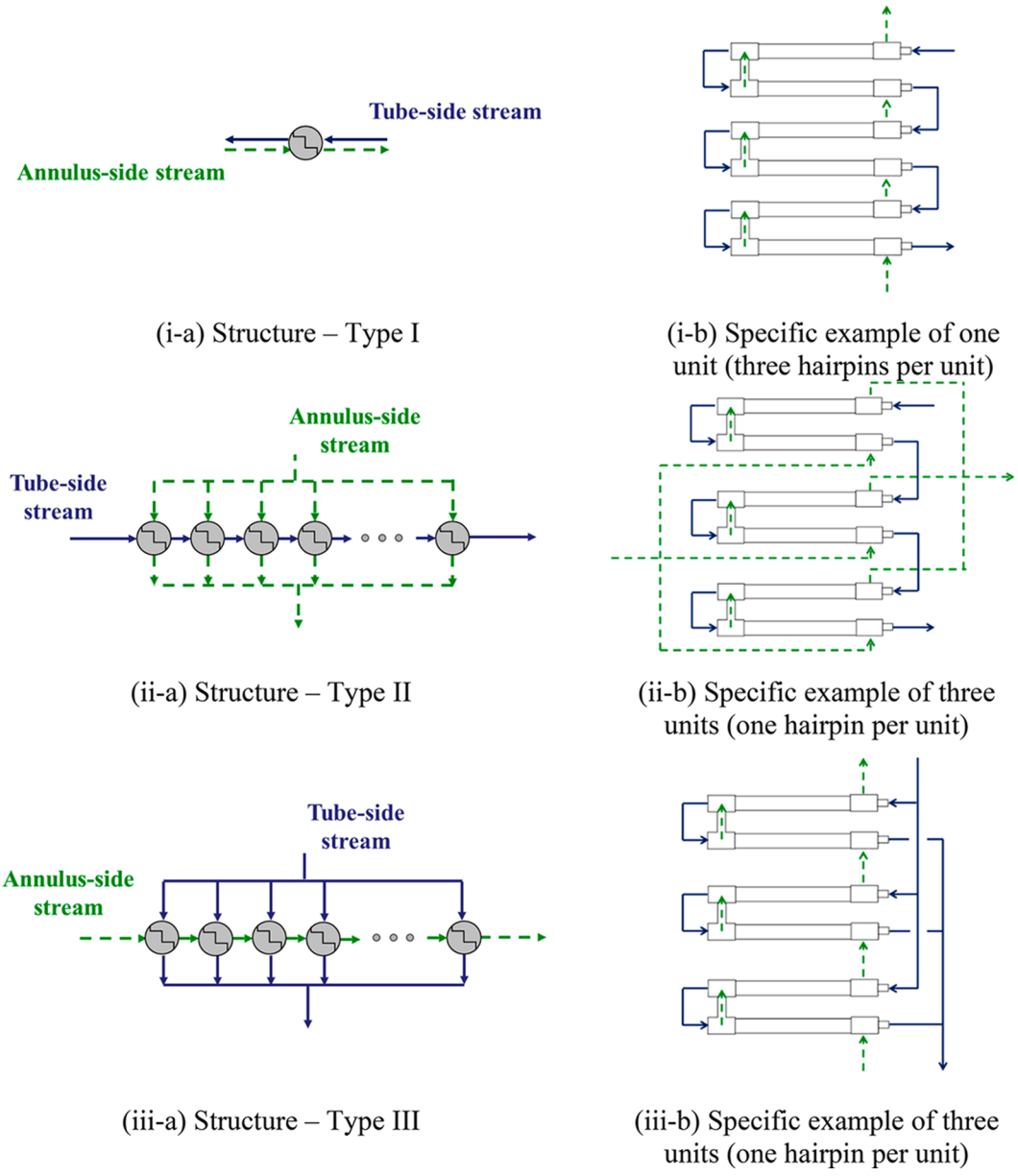

Figure 4. Arrangements. (i) Type I, streams aligned in series; (ii) Type II, tube-side stream aligned in series and annulus-side stream in parallel; (iii) Type III, annulus-side stream in series and tube-side stream in parallel. (a) Generic representation; (b) specific examples.

- unit: multiple hairpins connected in series (Figure 3 shows an example of a unit of two hairpins)
- branch: A structure composed of units that can be arranged in three different ways, as illustrated in Figure 4: (i) tube-side and annulus-side streams aligned in series, (ii) tube-side stream aligned in series and annulus-side stream aligned in parallel, and (iii) tube-side stream aligned in parallel and annulus-side stream in series
- general structure: The association of one of the structures shown in Figure 4 in a set of parallel branches, as illustrated by Figure 5 for the tube-side stream aligned in parallel and annulus-side stream in series.

The design problem involves the determination of the following:

- stream allocation of the hot and cold streams (tube-side or annulus-side)
- diameter and length of the tubes of the heat exchanger hairpins (all hairpins are equal)
- layout (number of hairpins per unit, number of units in parallel for each flow side per branch and the number of branches)

The traditional heat exchanger design equations (LMTD method and Darcy–Weisbach equation) are employed, minimizing the total heat transfer area, constrained by maximum allowed pressure drops. Finally, it is only considered streams without phase change and constant physical properties (representing average values), but considering any flow regime (laminar, transitional, and turbulent). The LMTD method uses a logarithmic mean temperature difference given by inlet and outlet temperatures of counterflow patterns. Although in Figure 4 each unit corresponds to a number of hairpins of counter-current flow, the overall flow pattern in Figure 4, (ii) and (iii) does not correspond to a true countercurrent flow. To account

DOI: 10.1021/acs.iecr.9b01536
Ind. Eng. Chem. Res. 2019, 58, 12080–12096

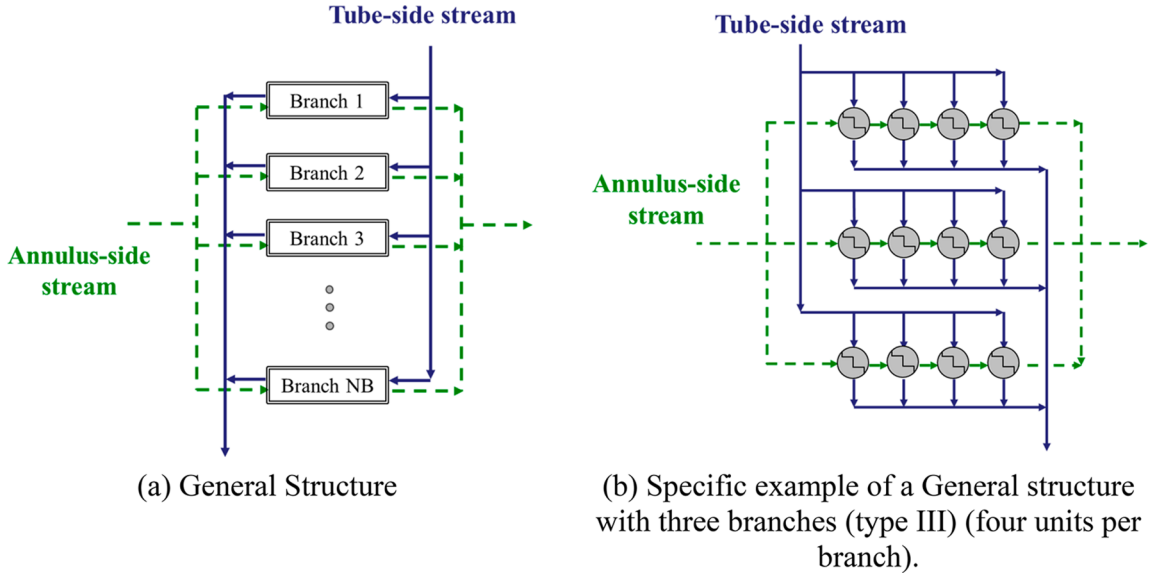

(a) General Structure

(b) Specific example of a General structure with three branches (type III) (four units per branch).

Figure 5. Double pipe heat exchanger general structure with multiple parallel branches: (a) generic representation; (b) three type III parallel branches of four units.

for the deviation of the internal flow pattern from that of a countercurrent flow, the logarithmic mean temperature difference is multiplied by a correction factor. This factor starts at 1 for pure countercurrent flow and reduces its value as the number of units per branch increases. Because the factor is obtained analytically, it is a rigorous correction and therefore does not change the accuracy of the formulation.

3. MODEL FORMULATION

The problem constraints are composed of the representation of the geometric variables, stream allocation equations, structural constraints, thermal and hydraulic modeling, and pressure drop and velocity bounds. The problem parameters that are kept constant during the optimization, are identified with a symbol ∧ on top.

3.1. Discrete Representation of Geometric Variables.

The diameter and length of the tubes employed in the construction of the heat exchanger are usually selected from a set of discrete values according to the available standard options. This design feature imposes the following relations involving the sets of binary variables that represent the available options:

$$dte = \sum_{sd=1}^{sd\max} \widehat{pdte}_{sd}\, yd_{sd} \tag{1}$$

$$dti = \sum_{sd=1}^{sd\max} \widehat{pdti}_{sd}\, yd_{sd} \tag{2}$$

$$Dte = \sum_{sD=1}^{sD\max} \widehat{pDte}_{sD}\, yD_{sD} \tag{3}$$

$$Dti = \sum_{sD=1}^{sD\max} \widehat{pDti}_{sD}\, yD_{sD} \tag{4}$$

$$Lh = \sum_{sL_h=1}^{sL_h\max} \widehat{pLh}_{sLh}\, yLh_{sLh} \tag{5}$$

$$\sum_{sd=1}^{sd\max} yd_{sd} = 1 \tag{6}$$

$$\sum_{sD=1}^{sD\max} yD_{sD} = 1 \tag{7}$$

$$\sum_{sLh=1}^{sLh\max} yLh_{sLh} = 1 \tag{8}$$

where dte and dti are the outer and inner diameters of the inner tube, Dte and Dti are the outer and inner diameters of the outer tube, and Lh is the tube length of each hairpin. The corresponding binary variables which indicate the discrete options selected are yd_{sd} for the inner tube diameter (discrete values: $\widehat{pdte}_{sd}$ and $\widehat{pdti}_{sd}$), yD_{sD} for the outer tube diameter (discrete values: $\widehat{pDte}_{sD}$ and $\widehat{pDti}_{sD}$), and yLh_{sLh} for the tube length (discrete values: $\widehat{pLh}_{sLh}$).

The selection of the number of parallel branches present in the heat exchanger design (NB) is represented by the binary variables yB_{sB}:

$$NB = \sum_{sB=1}^{sB\max} \widehat{pNB}_{sB}\, yB_{sB} \tag{9}$$

$$\sum_{sB=1}^{sB\max} yB_{sB} = 1 \tag{10}$$

where $\widehat{pNB}_{sB}$ is the set of discrete values of the possible number of parallel branches (1, 2, ..., sBmax).

The number of units aligned in parallel in each branch for the tube-side stream (NPt) and for the annulus-side stream (NPa) as well as the number of countercurrent hairpins per unit (Nh) are also represented using binary variables according to their integer nature:

DOI: 10.1021/acs.iecr.9b01536
Ind. Eng. Chem. Res. 2019, 58, 12080−12096

$$NPt = \sum_{sE=1}^{sE\max} \widehat{pNE}_{sE} yPt_{sE} \tag{11}$$

$$NPa = \sum_{sE=1}^{sE\max} \widehat{pNE}_{sE} yPa_{sE} \tag{12}$$

$$Nh = \sum_{sNh=1}^{sNh\max} \widehat{pNh}_{sNh} yNh_{sNh} \tag{13}$$

$$\sum_{sE=1}^{sE\max} yPt_{sE} = 1 \tag{14}$$

$$\sum_{sE=1}^{sE\max} yPa_{sE} = 1 \tag{15}$$

$$\sum_{sNh=1}^{sNh\max} yNh_{sNh} = 1 \tag{16}$$

where yPt_{sE} and yPa_{sE} are the binary variables which represent the integer options of the number of units in parallel per branch for the tube-side and the annulus-side streams, and $\widehat{pNE}_{sE}$ is the sequence of integer numbers representing the possible numbers of units interconnected along a branch (1, 2, ..., sE_{max}). For branch structure type I (Figure 4i-a) the number of parallel units selected for both flow-sides (NPt and NPa) are equal to unity ($yPt_{sE=1} = yPa_{sE=1} = 1$). Similarly, yNh_{sNh} is the binary variable that represent the integer options of the number of hairpins per unit, and $\widehat{pNh}_{sNh}$ is the sequence of integer numbers representing the number of hairpins possible per unit (1, 2, ..., sNh_{max}).

According to the structural options shown in Figure 4, an additional constraint must be included to ensure that if the tube-side has already more than one parallel passage, the annular side can be only arranged in series and vice versa:

$$yPt_{sE=1} + yPa_{sE=1} \geq 1 \tag{17}$$

To force that the outer tube inner diameter is larger than the inner tube outer diameter one writes:

$$\sum_{sD=1}^{sD\max} \widehat{pDti}_{sD} yD_{sD} \geq \sum_{sd=1}^{sd\max} \widehat{pdte}_{sd} yd_{sd} + \varepsilon \tag{18}$$

where ε is the smallest diameter difference. Alternatively, one can construct the model where each equation containing both diameters is written only for combinations (sd,sD)* that are allowed. This latter option is favored when sets can be used in programming environments such as GAMS.

The utilization of the proposed set of binary variables to describe the interconnection structure of double pipe heat exchanger elements is illustrated by the example depicted in Figure 6. According to the proposed approach, the nonzero binary variables that describe the structure presented in this figure are $yB_{sB=3} = 1$ (three parallel branches), $yPt_{sE=1} = 1$ and $yPa_{sE=5} = 1$ (five units per branch aligned in series for the tube-side flow and in parallel for the annulus-side flow) and $yNh_{sNh=2} = 1$ (two hairpins per branch).

3.2. Stream Allocation. The stream allocation is controlled by the binary variables yT_c and yT_h. If $yT_c = 1$, then the cold stream flows inside the inner tube and the hot stream flows in the annulus; if $yT_h = 1$, then the hot stream flows inside the inner tube and the cold stream flows in the annulus.

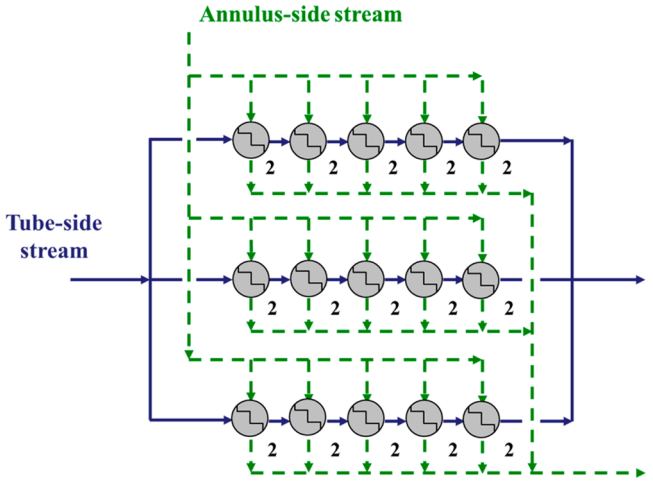

Figure 6. General structure of three parallel branches ($yB_{sB=3} = 1$).

One may associate known parameters of the hot and cold streams, such as mass flow rates ($\widehat{m}_h$ and $\widehat{m}_c$), for instance, to the corresponding variables for the tube-side and annulus-side flows:

$$mt = \widehat{m}_c yT_c + \widehat{m}_h yT_h \tag{19}$$

$$ma = \widehat{m}_c yT_h + \widehat{m}_h yT_c \tag{20}$$

Thus, if the cold stream flows inside the inner tube ($yT_c = 1$), then $mt = \widehat{m}_c$ and $ma = \widehat{m}_h$. Analogously, the following equations relate physical properties and fouling factors of the hot and cold streams to the corresponding values of the tube-side and annulus-side flows:

$$\rho t = \hat{\rho}_c yT_c + \hat{\rho}_h yT_h \tag{21}$$

$$\rho a = \hat{\rho}_c yT_h + \hat{\rho}_h yT_c \tag{22}$$

$$Cpt = \widehat{Cp}_c yT_c + \widehat{Cp}_h yT_h \tag{23}$$

$$Cpa = \widehat{Cp}_c yT_h + \widehat{Cp}_h yT_c \tag{24}$$

$$\mu t = \hat{\mu}_c yT_c + \hat{\mu}_h yT_h \tag{25}$$

$$\mu a = \hat{\mu}_c yT_h + \hat{\mu}_h yT_c \tag{26}$$

$$kt = \hat{k}_c yT_c + \hat{k}_h yT_h \tag{27}$$

$$ka = \hat{k}_c yT_h + \hat{k}_h yT_c \tag{28}$$

$$Rft = \widehat{Rf}_c yT_c + \widehat{Rf}_h yT_h \tag{29}$$

$$Rfa = \widehat{Rf}_c yT_h + \widehat{Rf}_h yT_c \tag{30}$$

$$yT_c + yT_h = 1 \tag{31}$$

where m is the mass flow rate, ρ is the density, Cp is the heat capacity, μ is the viscosity, k is the thermal conductivity, Rf is the fouling factor, and the subscripts c and h indicate the cold and hot streams, respectively.

3.3. Structural Constraints. The flow area and length of the hydraulic path of the streams considering the complete double pipe heat exchanger structure depend on the selection of the

DOI: 10.1021/acs.iecr.9b01536
Ind. Eng. Chem. Res. 2019, 58, 12080−12096

tube diameters and length, the number of hairpins and units in series and in parallel in each branch, and the number of parallel branches:

$$At = \left(\frac{\pi dti^2}{4}\right) NB\ NPt \tag{32}$$

$$Aa = \left(\frac{\pi Dti^2}{4} - \frac{\pi dte^2}{4}\right) NB\ NPa \tag{33}$$

$$Lu = Nh\ Lh \tag{34}$$

$$Lt = Lu\ NPa \tag{35}$$

$$La = Lu\ NPt \tag{36}$$

where At and Aa are the tube-side and annulus-side flow area, Lu is the total length of one unit and Lt and La are the corresponding flow path lengths for the streams flowing in the inner tube and in the annulus, respectively.

3.4. Inner Tube Side Thermal and Hydraulic Modeling.

The Prandtl number is given by

$$Prt = \frac{Cpt\ \mu t}{kt} \tag{37}$$

The flow velocity and the corresponding Reynolds number are given by

$$vt = \frac{(mt/\rho t)}{At} \tag{38}$$

$$Ret = \frac{dti\ vt\ \rho t}{\mu t} \tag{39}$$

Ignoring the minor head losses in the connections and bends, the pressure drop of the flow in the inner tube is calculated by the Darcy–Weisbach equation (omitting the viscosity correction factor):[15]

$$\Delta Pt = \rho t\ ft \frac{Lt}{dti} \frac{vt^2}{2} \tag{40}$$

where ft is the Darcy friction factor.

The friction factor depends on the flow regime as follows:[15]

$$ft^{\text{lam}} = \frac{64}{Ret} \quad \text{for } Ret \le 1311 \tag{41}$$

$$ft^{tran} = 0.0488 \quad \text{for } 1311 < Ret \le 3380 \tag{42}$$

$$ft^{\text{turb}} = 0.014 + \frac{1.056}{Ret^{0.42}} \quad \text{for } Ret > 3380 \tag{43}$$

The values of the intervals of the different flow regimes in eqs 41 to 43 guarantee a continuous profile of the friction factor, as shown in Figure 7.

Regarding the Nusselt number; laminar, transitional, and turbulent flows are considered, with the threshold of $Ret = 2300$ between the laminar and the transitional/turbulent flow. For the transitional and turbulent flow, the Gnielinski correlation is used:[16]

$$Nut^{\text{Gni}} = \frac{(ft/8)(Ret - 1000)Prt}{1 + 12.7(ft/8)^{1/2}(Prt^{2/3} - 1)} \quad \text{for } Ret > 2300 \tag{44}$$

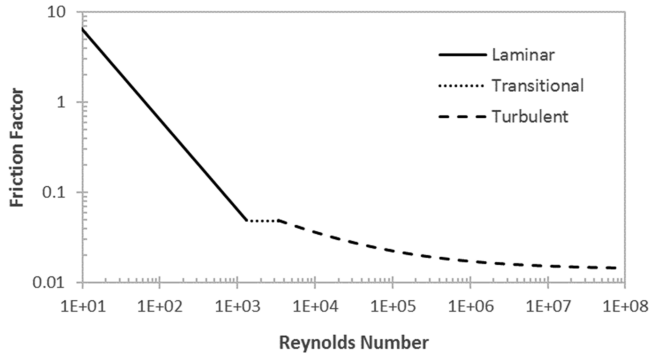

Figure 7. Inner tube friction factor profile in all regimes generated from eqs 41–43.

Since the laminar flow is more affected by the entry region, more than one equation is utilized, according to the proposal of Incropera et al.[16] For $Prt > 5$, the Hausen correlation is used:

$$Nut^{\text{Hau}} = 3.66 + \frac{0.0668(2dti/Lh)Ret\ Prt}{1 + 0.04((2dti/Lh)Ret\ Prt)^{2/3}}$$
$$\text{for } Ret \le 2300;\ Prt > 5 \tag{45}$$

For $Prt \le 5$, the Nusselt number is specified by the Sieder and Tate (S&T) correlation unless its given value is lower than the theoretical (theo) Nusselt number for fully developed flow (3.66), in which case the latter is applied:

$$Nut^{\text{S\&T}} = 1.86\left(\frac{Ret\ Prt\ dti}{Lh/2}\right)^{1/3}$$
$$\text{for } Ret \le 2300,\ Prt \le 5,\ Nut^{\text{S\&T}} \ge 3.66 \tag{46}$$

$$Nut^{\text{theo}} = 3.66 \quad \text{for } Ret \le 2300,\ Prt \le 5,\ Nut^{\text{S\&T}} < 3.66 \tag{47}$$

Without loss of generality, the viscosity correction factor in the Sieder and Tate correlation in eq 46 has also been omitted (i.e., the ratio between bulk and wall viscosities were considered equal to 1).

To formulate a set of constraints able to represent the friction factor and Nusselt number evaluation for all possible conditions described in eqs 41 to 47, binary variables are associated with the possible ranges of Ret, Prt, and Nut, as indicated in Figure 8. In this figure, $\widehat{URe}$, $\widehat{UPr}$, and $\widehat{UNu}$ are maximum values of Re, Pr, and Nu, respectively. In each interval, the corresponding binary variable is equal to 1 and the others are 0.

The following equations relate the binary variables and their corresponding ranges:

$$Ret \le 1311 yRet_1 + 2300 yRet_2 + 3380 yRet_3 + \widehat{URe}\ yRet_4 \tag{48}$$

$$Ret \ge 1311 yRet_2 + 2300 yRet_3 + 3380 yRet_4 + \varepsilon \tag{49}$$

$$Prt \le 5 yPrt_1 + \widehat{UPr}\ yPrt_2 \tag{50}$$

$$Prt \ge 5 yPrt_2 + \varepsilon \tag{51}$$

$$Nut^{\text{S\&T}} \le 3.66 yNut_1 + \widehat{UNu}\ yNut_2 - \varepsilon \tag{52}$$

$$Nut^{\text{S\&T}} \ge 3.66 yNut_2 \tag{53}$$

where ε is a small positive number.

DOI: 10.1021/acs.iecr.9b01536
Ind. Eng. Chem. Res. 2019, 58, 12080–12096

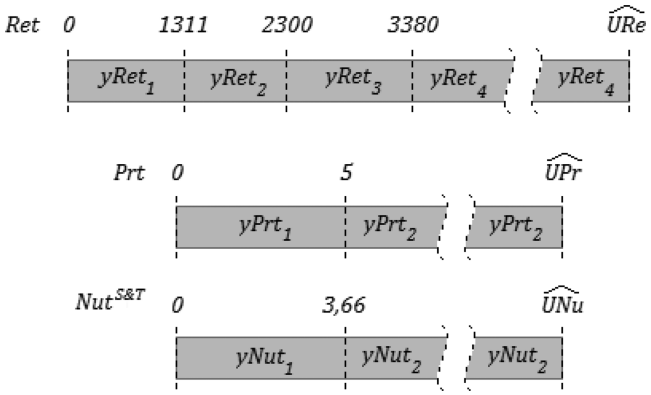

Figure 8. Possible ranges for *Ret*, *Prt*, $Nut^{S\&T}$ and its corresponding binary variables.

Since only one binary variable must be selected for each set of intervals, it yields

$$\sum_{sRet=1}^{sRet\max} yRet_{sRet} = 1 \tag{54}$$

$$yPrt_1 + yPrt_2 = 1 \tag{55}$$

$$yNut_1 + yNut_2 = 1 \tag{56}$$

Therefore, the friction factor and the Nusselt number are represented by

$$ft = ft^{lam} yRet_1 + ft^{tran}(yRet_2 + yRet_3) + ft^{turb} yRet_4 \tag{57}$$

$$\begin{aligned} Nut = {} & Nut^{theo}(yRet_1 + yRet_2)yPrt_1\, yNut_1 \\ & + Nut^{S\&T}(yRet_1 + yRet_2)yPrt_1\, yNut_2 \\ & + Nut^{Hau}(yRet_1 + yRet_2)yPrt_2 \\ & + Nut^{Gni}(yRet_3 + yRet_4) \end{aligned} \tag{58}$$

3.5. Annulus Side Thermal and Hydraulic Modeling.

The Prandtl number is

$$Pra = \frac{Cpa\ \mu a}{ka} \tag{59}$$

The flow velocity inside the annular region is given by

$$va = \frac{(ma/\rho a)}{Aa} \tag{60}$$

The hydraulic diameter (four times the flow cross-sectional area divided by the wetted perimeter) can be simplified to[16]

$$dh = Dti - dte \tag{61}$$

The Reynolds number is

$$Rea = \frac{dh\ va\ \rho a}{\mu a} \tag{62}$$

Ignoring the head losses in the connections and bends, the pressure drop of the flow in the annulus is given by the Darcy–Weisbach equation using the hydraulic diameter (also omitting the viscosity correction factor):[15]

$$\Delta Pa = \rho a\, fa \frac{Lt}{dh} \frac{va^2}{2} \tag{63}$$

where *fa* is the Darcy friction factor for the annular flow.

The annular region friction factor, analogously to the inner tube, depends on the flow regime according to the following equations:[15]

$$fa^{lam} = \frac{64}{Rea} \quad \text{for } Rea \le 500 \tag{64}$$

$$fa^{tran} = 0.02696 + \frac{32.656}{Rea^{0.93}} \quad \text{for } 500 < Rea \le 10000 \tag{65}$$

$$fa^{turb} = \frac{0.178}{Rea^{0.1865}} \quad \text{for } Rea > 10000 \tag{66}$$

The threshold Reynolds number values in this case are 500 and 10000 and these equations also form a continuous profile for calculation of the friction factor, as shown in Figure 9.

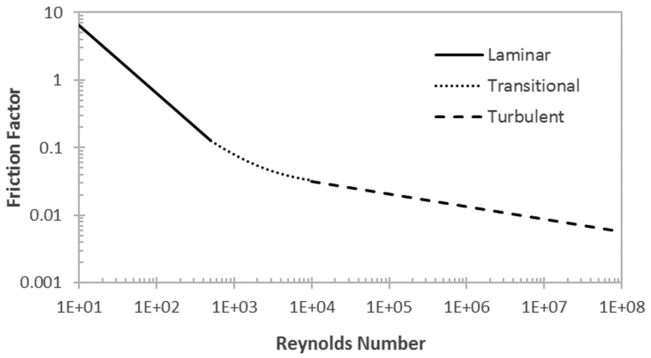

Figure 9. Annular friction factor profile in all three regimes generated from eqs 64–66.

Regarding the Nusselt number, the same ranges and correlations used for the tube-side are applied, replacing the inner tube diameter by the hydraulic diameter:

$$Nua^{theo} = 3.66 \quad \text{for } Rea \le 2300,\ Pra \le 5,\ \text{and } Nua^{S\&T} < 3.66 \tag{67}$$

$$Nua^{S\&T} = 1.86\left(\frac{Rea\ Pra\ dh}{Lh/2}\right)^{1/3} \quad \text{for } Rea \le 2300,\ Pra \le 5 \text{ and } Nua^{S\&T} \ge 3.66 \tag{68}$$

$$Nua^{Hau} = 3.66 + \frac{0.0668(2dh/Lh)Rea\ Pra}{1 + 0.04((2dh/Lh)Rea\ Pra)^{2/3}} \quad \text{for } Rea \le 2300 \text{ and } Pra > 5 \tag{69}$$

$$Nua^{Gni} = \frac{(fa/8)(Rea - 1000)Pra}{1 + 12.7(fa/8)^{1/2}(Pra^{2/3} - 1)} \quad \text{for } Rea > 2300 \tag{70}$$

Binary variables are then included to describe each interval of *Rea*, *Pra*, and $Nua^{S\&T}$, as depicted in Figure 10. The same approach used for the tube-side flow for the evaluation of the Nusselt number is implemented here as follows:

$$Rea \le 500yRea_1 + 2300yRea_2 + 10000yRea_3 + \widehat{URe}\ yRea_4 \tag{71}$$

$$Rea \ge 500yRea_2 + 2300yRea_3 + 10000yRea_4 + \varepsilon \tag{72}$$

$$Pra \le 5yPra_1 + \widehat{UPr}\ yPra_2 \tag{73}$$

DOI: 10.1021/acs.iecr.9b01536
Ind. Eng. Chem. Res. 2019, 58, 12080–12096

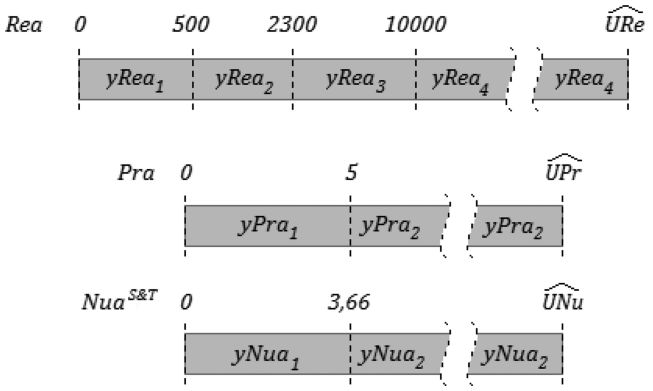

Figure 10. Possible ranges for *Rea*, *Pra*, $Nua^{S\&T}$ and their corresponding binary variables.

$$Pra \geq 5yPra_2 + \varepsilon \tag{74}$$

$$Nua^{S\&T} \leq 3.66yNua_1 + \widehat{UNu}\, yNua_2 - \varepsilon \tag{75}$$

$$Nua^{S\&T} \geq 3.66yNua_2 \tag{76}$$

$$\sum_{sRea=1}^{sRea\max} yRea_{sRea} = 1 \tag{77}$$

$$yPra_1 + yPra_2 = 1 \tag{78}$$

$$yNua_1 + yNua_2 = 1 \tag{79}$$

$$fa = fa^{lam} yRea_1 + fa^{tran}(yRea_2 + yRea_3) + fa^{turb} yRea_4 \tag{80}$$

$$\begin{aligned} Nua = {} & Nua^{theo}(yRea_1 + yRea_2)yPra_1\, yNua_1 \\ & + Nua^{S\&T}(yRea_1 + yRea_2)yPra_1\, yNua_2 \\ & + Nua^{Hau}(yRea_1 + yRea_2)yPra_2 \\ & + Nua^{Gni}(yRea_3 + yRea_4) \end{aligned} \tag{81}$$

3.6. Heat Transfer Coefficients. The convective heat transfer coefficient for the tube-side and annulus-side flows are given by

$$ht = \frac{Nut\ kt}{dti} \tag{82}$$

$$ha = \frac{Nua\ ka}{dh} \tag{83}$$

The overall heat transfer coefficient is then determined by

$$U = \frac{1}{\frac{1}{ht}\frac{dte}{dti} + Rft\frac{dte}{dti} + \frac{dte\ \ln\left(\frac{dte}{dti}\right)}{2\widehat{ktube}} + Rfa + \frac{1}{ha}} \tag{84}$$

where $\widehat{ktube}$ is the thermal conductivity of the inner tube.

3.7. Heat Transfer Rate. The heat transfer rate is given by

$$\hat{Q} = UA_{req}\widehat{\Delta Tlm}\, F \tag{85}$$

where A_{req} is the required heat transfer area, $\widehat{\Delta Tlm}$ is the logarithmic mean temperature, and F is the correction factor.

The logarithmic mean temperature is defined as

$$\widehat{\Delta Tlm} = \frac{(\widehat{Ti_h} - \widehat{To_c}) - (\widehat{To_h} - \widehat{Ti_c})}{\ln\left(\frac{(\widehat{Ti_h} - \widehat{To_c})}{(\widehat{To_h} - \widehat{Ti_c})}\right)} \tag{86}$$

where $\widehat{Ti_h}$ and $\widehat{To_h}$ are the inlet and outlet temperatures of the hot stream, and $\widehat{Ti_c}$ and $\widehat{To_c}$ are the inlet and outlet temperatures of the cold stream.

As discussed above, the correction factor depends on the structure of the arrangement of the double pipe heat exchanger units. If the structure is based on an arrangement where both streams are aligned in series, (type I, as shown in Figure 4i-a), the correction factor is equal to unity. If the structure has one of the streams in parallel, as in branch structures of type II (Figure 4ii-a and type III (Figure 4iii-a), its value depends on which stream is in parallel and on the number of existing units per branch.[13] As the number of units in parallel increases the correction factor decreases, accounting for the deviation from a countercurrent flow pattern. The number of hairpins per unit and the number of parallel branches in the general structure do not implicate any flow pattern change between streams and therefore do not have any influence on the correction factor value. All the correction factor options are calculated as parameters prior to the optimization. For stream *sST* (cold, *sST* = c, or hot, *sST* = h) aligned in series and the other stream in parallel, the correction factor is given by[13]

$$\widehat{pF}_{sST,sE} = \frac{(\widehat{pR}_{sST} - \widehat{pNE}_{sE})}{\widehat{pNE}_{sE}(\widehat{pR}_{sST} - 1)} \frac{\ln\left(\frac{1-\widehat{pP}_{sST}}{1-\widehat{pP}_{sST}\widehat{pR}_{sST}}\right)}{\ln\left(\frac{\widehat{pR}_{sST} - \widehat{pNE}_{sE}}{\widehat{pR}_{sST}(1-\widehat{pP}_{sST}\widehat{pR}_{sST})^{1/\widehat{pNE}_{sE}}} + \frac{\widehat{pNE}_{sE}}{\widehat{pR}_{sST}}\right)} \quad \text{for } sE \neq 1 \tag{87}$$

where the factors $\widehat{pR}_{sST}$ and $\widehat{pP}_{sST}$ are specified as

$$\widehat{pR}_{sST} = \begin{cases} \dfrac{(\widehat{To_c} - \widehat{Ti_c})}{(\widehat{Ti_h} - \widehat{To_h})} & \text{for } sST = \text{c} \\ \dfrac{(\widehat{Ti_h} - \widehat{To_h})}{(\widehat{To_c} - \widehat{Ti_c})} & \text{for } sST = \text{h} \end{cases} \tag{88}$$

$$\widehat{pP}_{sST} = \begin{cases} \dfrac{(\widehat{Ti_h} - \widehat{To_h})}{(\widehat{Ti_h} - \widehat{Ti_c})} & \text{for } sST = \text{c} \\ \dfrac{(\widehat{To_c} - \widehat{Ti_c})}{(\widehat{Ti_h} - \widehat{Ti_c})} & \text{for } sST = \text{h} \end{cases} \tag{89}$$

On the basis of these expressions, the constraint that represents the correction factor (F) evaluation, dependent on the structure selected, becomes

$$\begin{aligned} F = 1 + \sum_{sE=2}^{sEmax}\sum_{sE'=2}^{sEmax} \{ & yT_c[yPt_{sE}(\widehat{pF}_{h,sE} - 1) \\ & + yPa_{sE,}(\widehat{pF}_{c,sE,} - 1)] + yT_h[yPt_{sE}(\widehat{pF}_{c,sE} - 1) \\ & + yPa_{sE,}(\widehat{pF}_{h,sE,} - 1)]\} \end{aligned} \tag{90}$$

In turn, aiming at guaranteeing a design margin, a minimum area excess ($\hat{A}_{exc}$) is imposed.

$$A \geq \left(1 + \frac{\hat{A}_{exc}}{100}\right) A_{req} \tag{91}$$

DOI: 10.1021/acs.iecr.9b01536
Ind. Eng. Chem. Res. 2019, 58, 12080−12096

where the equipment heat transfer area is given by

$$A = \pi\ dte\ Lu\ NB\ NPt\ NPa \tag{92}$$

Therefore, the heat transfer rate shown in eq 85 can be reorganized as

$$UA \geq \frac{\hat{Q}\left(\frac{\widehat{A_{exc}}}{100} + 1\right)}{\widehat{\Delta Tlm}\ F} \tag{93}$$

3.8. Pressure Drop and Velocity Bounds. The lower and upper bounds on the velocities of the tube-side flow and annulus-side flow are given by

$$vt \geq \widehat{vt}_{min} \tag{94}$$

$$vt \leq \widehat{vt}_{max} \tag{95}$$

$$va \geq \widehat{va}_{min} \tag{96}$$

$$va \leq \widehat{va}_{max} \tag{97}$$

While the pressure drop bounds are represented by

$$\Delta Pt \leq \widehat{\Delta P_{c_{disp}}} yT_c + \widehat{\Delta P_{h_{disp}}} yT_h \tag{98}$$

$$\Delta Pa \leq \widehat{\Delta P_{c_{disp}}} yT_h + \widehat{\Delta P_{h_{disp}}} yT_c \tag{99}$$

3.9. Objective Function. The objective function is given by the minimization of the heat transfer area:

$$\min A + \widehat{ph}\ Nh \tag{100}$$

where ph is a penalty factor (a random small value) associated with the number of hairpins directing the optimization, in case of equivalent solutions, to the one with the smaller number of elements.

The above model is here called the raw MINLP. It uses a discrete representation of the geometric variables and several nonlinear relationships involving continuous variables. Additionally, some equations contain nonlinearities involving binary variables (eqs 57, 58, 80, 81, and 90), that are incompatible with the use of some optimization algorithms.

To make the model more amenable to be solved by algorithms that require linearity in binary variables, a reformulation to obtain another mixed-integer nonlinear model linear in the binaries is also presented, resulting in what is here called binary-linear MINLP.

4. MINLP REFORMULATION

This section presents the reformulation of some constraints to eliminate the nonlinearities involving binary variables (thus rendering the binary-linear MINLP model). The linear constraints or the constraints with continuous-only nonlinearities remain the same.

4.1. Reformulation Techniques. In the original optimization problem (raw MINLP model), there are two types of nonlinear terms involving binaries: the product of two or more binary variables and the product of a binary variable and a function of continuous variables.

The product of binary variables can be substituted by a continuous variable and a set of linear inequalities, as follows.[17]

Let yp_i, yq_j, ..., and yz_k be a set of binary variables. The product of these variables can be substituted by a continuous nonnegative variable $w_{i,j,\cdots,k}$:

$$w_{i,j,\ldots,k} = yp_i\ yq_j \ldots yz_k \tag{101}$$

where this equality is guaranteed by the inclusion of these constraints:

$$w_{i,j,\ldots,k} \leq yp_i \tag{102}$$

$$w_{i,j,\ldots,k} \leq yq_j \tag{103}$$

$$\ldots$$

$$w_{i,j,\ldots,k} \leq yz_k \tag{104}$$

$$w_{i,j,\ldots,k} \geq yp_i + yq_j + \ldots + yz_k - (m-1) \tag{105}$$

where m is the number of binary variables in the product.

The reformulation of the product between a binary variable and a function of continuous variables also involves the introduction of an additional continuous variable and a set of inequality constraints.[17]

Let $f(x_1, x_2, \ldots)$ be a function of continuous variables such that $0 \leq f \leq \hat{\Phi}$ in the problem domain and y is a binary variable. The product of this function and the binary variable can be substituted by a continuous nonnegative variable w together with the inclusion of these constraints:

$$w - \hat{\Phi}\ y \leq 0 \tag{106}$$

$$f(x_1, x_2, \ldots) - w - \hat{\Phi}(1-y) \leq 0 \tag{107}$$

$$f(x_1, x_2, \ldots) - w \geq 0 \tag{108}$$

4.2. Resultant Formulation. The application of the approach described above modifies the following set of constraints: inner tube side thermal and hydraulic modeling, annulus side thermal and hydraulic modeling, and heat transfer rate. The detailed description of each equation modified is described in the Supporting Information.

5. HEURISTIC APPROACH

To later compare our MINLP approach to some heuristic approach, a proposal of a heuristic design procedure is presented here. Unlike for other equipment (i.e., distillation trays) there is no step-by-step heuristic procedure widely available in the literature (i.e., the identification of a feasible solution depends entirely on the intervention of the designer using a trial and verification method). Serth,[13] for example applies a trial-and-viability-verification without outlining any rule. Thus, his example is used here as a simple source to propose one such procedure. The proposed procedure is as follows:

- Assume a starting structure, as simple as possible. A good candidate is a one-unit branch structure as in Figure 4i-a.
- Pick hairpin dimensions from the discrete available options (diameters and length).
- Calculate the heat transfer coefficient, the required area (which together with a reasonable excess area, e.g., minimum of 10%, gives the necessary number of hairpins for the selected structure), and pressure drops.
- If the results meet the design requirements (e.g., velocities and pressure drops according to acceptable values) the procedure stops.
- Otherwise, a structure change is made, a step that is highly dependent on the designer, who, according to the unmet requirement, can (a) change fluid allocation, (b) change the hairpin dimensions (diameters and length), (c) select

DOI: 10.1021/acs.iecr.9b01536
Ind. Eng. Chem. Res. 2019, 58, 12080−12096

more or less branches, or (d) select another branch structure (Figure 4).

Quite clearly, some changes, such as dimensions, are the obvious first target: for example, if the area is smaller than the area required, and the pressure drop is lower than the limit, increasing length may be the first thing to consider. If pressure drop is the limiting factor, the obvious dimension to modify is the diameter, or the number of branches. The analysis of all the starting options and the decisions to make when the service requirements are not met, which would be in the direction of creating a rule-based automatic algorithm, is not pursued here.

6. RESULTS

Three aspects are explored in the analysis of the results:

Table 1. Initial Estimates for Key Binary Variables

variable	initial estimate
inner tube diameter selection	$yd_3 = 1$
stream allocation	$yT_c = 1$
range of Reynolds identification	$yRet_4 = yRea_4 = 1$
range of Nusselt identification	$yNut_2 = yNua_2 = 1$

Table 2. Initial Estimates for Key Continuous Variables

variable	initial estimate
length of one unit	$Lh = \frac{Lh_{lo} + Lh_{up}}{2}$
Reynolds number[a]	$Rex = \frac{Rex_{lo} + Rex_{up}}{2}$
Nusselt number[a]	$Nux = \frac{Nux_{lo} + Nux_{up}}{2}$
Seider and Tate Nusselt number[a]	$Nux^{S\&T} = \frac{Nux_{lo}^{S\&T} + Nux_{up}^{S\&T}}{2}$
Hausen Nusselt number	$Nut^{Hau} = 3.66$
	$Nua^{Hau} = 3.66$

[a] x being t (tube side) or a (annulus side).

Table 3. Example 1: Stream Data

parameter	unit	cold stream (benzene)	hot stream (aniline)
mass flow, $\hat{m}_{sST}$	kg/s	1.26	1.22
inlet temp, $\widehat{Ti}_{sST}$	°C	15.55	65.55
outlet temp, $\widehat{To}_{sST}$	°C	48.85	37.75
density, $\hat{\rho}_{sST}$	kg/m^3	879	1022
viscosity, $\hat{\mu}_{sST}$	Pa·s	5.5×10^{-4}	2×10^{-3}
heat capacity, $\widehat{Cp}_{sST}$	J/(kg °C)	1758.46	2177.14
thermal conductivity $\hat{k}_{sST}$	W/(m °C)	0.159	0.173
fouling resistance, $\widehat{Rf}_{sST}$	m^2 °C/W	1.76×10^{-4}	1.76×10^{-4}
available pressure drop, $\widehat{\Delta P}_{sST_{disp}}$	kPa	138	138

i. comparison of the mathematical programming solution with a result from the literature
ii. comparison of the mathematical programming solution with a solution generated by the procedure explained in section 5
iii. comparison between the proposed MINLP approaches

Complementarily, the Supporting Information material contains additional examples that explore the flexibility of the proposed approach in relation to different flow regimes and structural alternatives.

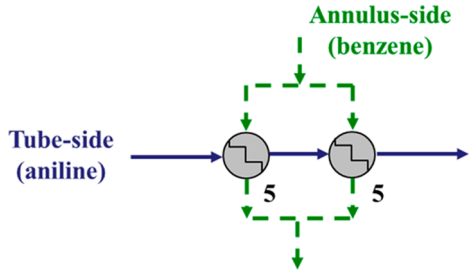

Figure 11. Example 1, heat exchanger structure obtained by Serth.[13]

The results explored in sections 6.1 and 6.2 are generated by our raw MINLP formulation, which is then compared with our linear-binary MINLP approach in section 6.3. All numerical results were obtained using the GAMS software version 23.7.3 and a branch-and-bound solver (SBB). Without good initial estimates, the SBB solver used does not converge for neither MINLP models. The result of the root node relaxation of the SBB solver is highly sensitive to the initial estimate. Thus, it was necessary to identify a suitable initial set of values for some of the problem variables to have convergence. GAMS default initial value for all variables is zero, unless zero is not within the bounded range (in which case the default is the bound closest to zero) or the user determines otherwise. Six binary variables were identified related to tube diameter, stream allocation, and range of Reynolds numbers that, in our examples, need initial values to promote the convergence. The values shown in Table 1 are the ones found to work well for the set of proposed examples for this set of variables. Furthermore, it was found that when using SBB, the convergence also depends on the initial estimate for some continuous variables, as shown in Table 2. Finally, DICOPT does not provide results for any of the two MINLP approaches, no matter what initial values are provided. This issue on initialization is not investigated further, because it is not the aim of the current paper to seek a general systematic route to find robust and automatic initialization procedures. Rather, all the difficulties associated with the use of local solvers are simply pointed out and these are difficulties known to many.

6.1. Comparison with Literature Results. Example 1 is a design problem proposed by Serth,[13] which consists of determining the number of required hairpins and their arrangement for the service shown in Table 3.

The design methodology employed by Serth[13] consists of a trial-and-viability-verification procedure, similar to the one shown in section 5. Serth[13] does not provide rules or hints of how to obtain a different design and stops its procedure when the first viable equipment is found.

The solution obtained by Serth[13] is illustrated in Figure 11 and consists in a single branch of type II structure (Figure 4ii-a), with an inner pipe stream connected in series and annulus side stream aligned in parallel in two units, each containing five hairpins using pipes with a thermal conductivity of 16.27 W/(m °C).

The thermo-fluid dynamic relations used by Serth[13] are different from the model employed in this paper, particularly the friction factor and the Nusselt number correlations. For comparison, Serth's correlations are used in the optimization applied to this example. Details of the resultant formulation using Serth's correlations employed in this example are shown in the Supporting Information material. In all other examples, the correlations presented in section 3 are employed.

DOI: 10.1021/acs.iecr.9b01536
Ind. Eng. Chem. Res. 2019, 58, 12080−12096

Table 4. Structural Discrete Options (Pipe Schedule 40)

parameter[a]	units	discrete options								
$\widehat{pNB}_{sB}$		1 to 20								
$\widehat{pNE}_{sE}$		1 to 20								
$\widehat{pLh}_{sLh}$	ft	5	10	15	20	25	32[b]			
$\widehat{pLh}_{sLh}$	m	1.524	3.048	4.572	6.096	7.620	9.75[b]			
inner tube NPS	in	1/2	3/4	1	1 1/4	1 1/2	2	2 1/2	3	3 1/2
inner tube OD ($\widehat{pdte}_{sd}$)	m	0.021	0.027	0.033	0.042	0.048	0.060	0.073	0.089	0.102
outer tube NPS	in	1 1/4	1 1/2	2	2 1/2	3	3 1/2	4	4 1/2	5
outer tube OD ($\widehat{pDte}_{sD}$)	m	0.042	0.048	0.060	0.073	0.089	0.102	0.114	0.127	0.168

[a]NPS = nominal pipe size, OD = outer diameter. [b]Option used only in section 6.1.

Table 5. Example 1: Results

variable[a]	units	Serth[13]	raw MINLP using Serth correlations	
			fixed geometry from Serth[13]	optimal solution
tube side stream		aniline	aniline	benzene
total heat exchanger area, *A*	m^2	12.91	12.92	9.96
required heat exchanger area	m^2	11.68	11.55	9.02
inner tube NPS−OD	in−m	1 1/4−0.042	1 1/4−0.042	3/4−0.027
outer tube NPS−OD	in−m	2−0.060	2−0.060	1 1/4−0.042
hairpin length, *Lh*	ft−m	32−9.75	32−9.75	10−3.048
number of hairpins per units, *Nh*		5	5	13
number of branches, *NB*		1	1	3
tube side units in parallel, *NPt*		1	1	1
annular side units in parallel, *NPa*		2	2	1
tube side velocity, *vt*	m/s	1.24	1.24	1.389
annulus side velocity, *va*	m/s	0.93	0.93	0.979
tube side film coefficient, *ht*	W/(m^2 °C)	999	996	1727
annulus side film coefficient, *ha*	W/(m^2 °C)	1448	1446	977
overall heat transfer coefficient, *U*	W/(m^2 °C)	391.8	395.9	423.8
correction factor, *F*		0.836	0.836	1
tube side pressure drop, *dPt*	kPa	82.0	78.9	49.0
annulus side pressure drop, *dPa*	kPa	70.3	71.1	123.5

[a]NPS = nominal pipe size, OD = outer diameter.

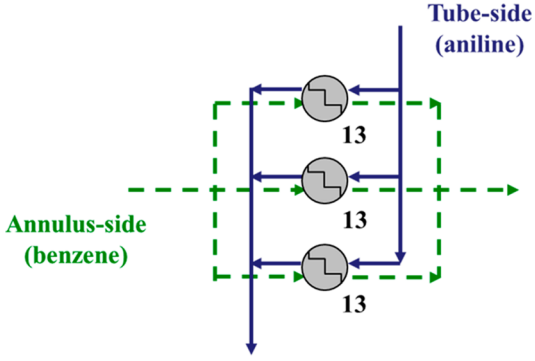

Figure 12. Example 1: Optimal solution obtained by our raw MINLP (with Serth correlations).

Additionally, it is also important to mention that the heat exchanger modeling employed in the optimization does not consider the pressure drops in the nozzles and return bends, and therefore these elements were excluded from the analysis. The results of pressure drop reported here from Serth[13] also excluded the head loss in these elements. An analysis of the trial-and-verification procedure adopted by Serth[13] indicates that the exclusion of these minor losses during the sequence of design

Table 6. Example 2: Stream Data

parameter	unit	cold stream	hot stream
mass flow, $\hat{m}_{sST}$	kg/s	2.52	2.11
inlet temperature, $\widehat{Ti}_{sST}$	°C	20	60
outlet temperature, $\widehat{To}_{sST}$	°C	30	50
density, $\hat{\rho}_{sST}$	kg/m^3	850	1000
viscosity, $\hat{\mu}_{sST}$	Pa·s	5.5×10^{-4}	2×10^{-4}
heat capacity, $\widehat{Cp}_{sST}$	J/(kg °C)	1760	2100
thermal conductivity $\hat{k}_{sST}$	W/(m °C)	0.160	0.175
fouling resistance, $\widehat{Rf}_{sST}$	m^2 °C/W	2×10^{-4}	2×10^{-4}

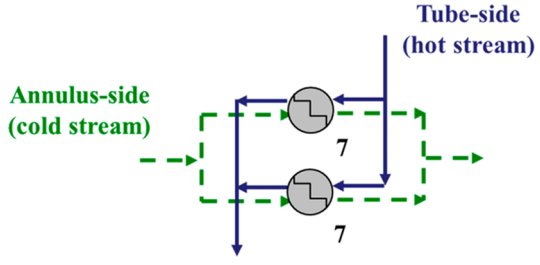

Figure 13. Example 2: Trial and verification procedure solution.

DOI: 10.1021/acs.iecr.9b01536
Ind. Eng. Chem. Res. 2019, 58, 12080−12096

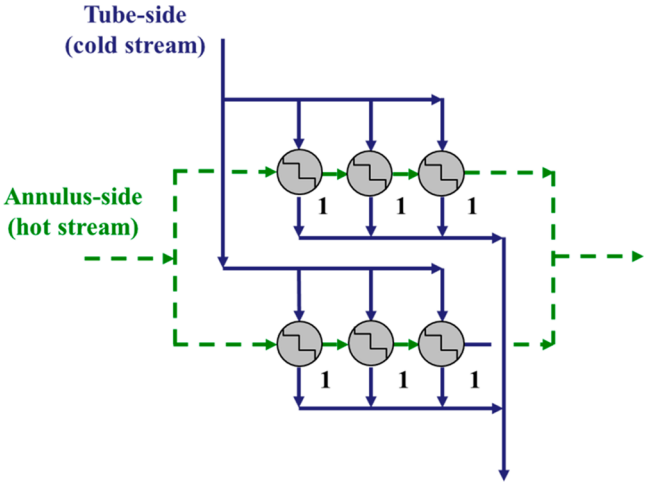

Figure 14. Example 2: Optimal solution obtained by our raw MINLP approach.

steps would not modify the result obtained, which enables a direct comparison of the results.

The optimization search space employed in the proposed analysis is depicted in Table 4, and includes the original design proposed by Serth.[13] The velocity bounds applied in the optimization runs were 0.9 to 3 m/s and a minimum excess area of 10% (same as used by Serth[13]). Also, for comparison purposes, the initial estimate was the first heat exchanger attempted by Serth in his trial-and-verification procedure, which consisted of a one countercurrent unit branch (structure on Figure 4i-a) with six hairpins (of the same dimensions as Serth's final solution) and benzene in the inner pipe. Table 5 contains the reported values by Serth,[14] the results obtained using the raw MINLP model modified to use Serth's correlations using the same geometry, and the corresponding optimal solution. The diameters for both inner and outer tubes are calculated considering pipe schedule 40.

The formulation proposed in this paper was able to find equivalent results from Serth[13] for the same heat exchanger structure (only the structural binary variables were fixed), therefore validating the model implemented. The small difference in the pressure drops were expected since Serth[13] accounts for the viscosity correction factor which is here omitted in eqs 40 and 63. Our optimization approach obtained an optimal result (illustrated in Figure 12) that shows a reduction of 23% in area, which is attained due to a combination of higher LMTD correction factor F resulting from the counter-current arrangement of the set of units of the proposed heat exchanger and a higher heat transfer coefficient resulting from a substantial improvement of the annulus heat transfer film coefficient, in turn enhanced by a higher velocity.

6.2. Comparison with Heuristic Approaches. The advantages of an MINLP approach over a heuristic trial-and-verification procedure are illustrated in example 1, originally solved by Serth.[13] For example 2, the stream data are depicted in Table 6.

The discrete options applied to this design problem are shown in Table 4, where a thermal conductivity of 55 W/(m °C) is used for the material of the pipes, flow velocity in both sides is between 1 and 3 m/s, available pressure drop for both streams is equal to 50 kPa, and there is a minimum excess area of 20%.

Heuristics shown in section 5 are used to obtain a viable solution, which is illustrated in Figure 13. The Supporting Information material depicts the steps taken during the procedure.

However, when using the raw MINLP formulation, one gets an area reduction of 17.8%, with the structure illustrated in Figure 14. This area reduction is achieved by using higher flow velocities compatible with available pressure drops (Table 7).

6.3. Comparison of the Performance of the MINLP Models. The two MINLP approaches are compared in this section. For examples 1 and 2, the optimization using the linear-binary MINLP formulation results in the same solutions as the ones from the raw MINLP formulation, already reported in the previous subsections. However, this is not a rule for every possible scenario, as illustrated here with examples 3 and 4, where both MINLP approaches give different results. The stream data for both examples are shown in Table 8. The

Table 7. Example 2: Design Results

variable[a]	unit	trial and verification	raw MINLP
tube side stream		hot stream	cold stream
total heat exchanger area, *A*	m^2	2.24	1.84
required heat exchanger area	m^2	1.79	1.51
inner tube NPS−OD	in−m	1−0.033	$^1/_2$−0.021
outer tube NPS−OD	in−m	2−0.060	$1^1/_4$−0.042
hairpin length, *Lh*	ft−m	5−1.52	15−4.572
number of hairpins per unit, *Nh*		7	1
number of branches, *NB*		2	2
tube side units in parallel, *NPt*		1	3
annular side units in parallel, *NPa*		1	1
tube side velocity, *vt*	m/s	1.89	2.52
annulus side velocity, *va*	m/s	1.15	1.74
tube side film coefficient, *ht*	W/(m^2°C)	6496	4292
annulus side film coefficient, *ha*	W/(m^2°C)	1995	6046
overall heat transfer coefficient, *U*	W/(m^2°C)	824	991.6
correction factor, *F*		1	0.989
tube side pressure drop, *dPt*	kPa	14.1	19.0
annulus side pressure drop, *dPa*	kPa	8.0	30.3

[a]NPS = nominal pipe size, OD = outer diameter.

DOI: 10.1021/acs.iecr.9b01536
Ind. Eng. Chem. Res. 2019, 58, 12080−12096

Table 8. Examples 3 and 4: Stream Data

		example 3		example 4	
parameter	unit	hot stream	cold stream	hot stream	cold stream
mass flow, $\hat{m}_{sST}$	kg/s	16.5	34.32	25.9	13.14
inlet temperature, $\widehat{Ti}_{sST}$	°C	90	30.1	60	10
outlet temperature, $\widehat{To}_{sST}$	°C	50	40	50	25
density, $\hat{\rho}_{sST}$	kg/m^3	786	995	780	1050
viscosity, $\hat{\mu}_{sST}$	Pa·s	1.89×10^{-4}	7.2×10^{-4}	9.5×10^{-4}	0.024
heat capacity, $\widehat{Cp}_{sST}$	J/(kg °C)	2177	4187	1900	2500
thermal conductivity $\hat{k}_{sST}$	W/(m °C)	0.12	0.59	0.18	0.264
fouling resistance, $\widehat{Rf}_{sST}$	m^2 °C/W	2×10^{-4}	4×10^{-4}	3×10^{-4}	3×10^{-4}
available pressure drop, $\widehat{\Delta P}_{sSTdisp}$	kPa	100	100	150	150

Table 9. Example 3: Optimization Results

variable	unit	raw MINLP	linear-binary MINLP
tube side stream		hot stream	hot stream
total heat exchanger area, *A*	m^2	88.73	91.15
required heat exchanger area	m^2	73.94	75.19
inner tube NPS−OD	in−m	1 $^1/_2$−0.048	1−0.033
outer tube NPS−OD	in−m	2 $^1/_2$−0.073	2−0.060
hairpin length, *Lh*	ft−m	20−6.096	25−7.620
number of hairpins per unit, *Nh*		6	6
number of branches, *NB*		8	19
tube side units in parallel, *NPt*		1	1
annular side units in parallel, *NPa*		2	1
tube side velocity, *vt*	m/s	2.00	1.98
annulus side velocity, *va*	m/s	1.71	1.41
tube side film coefficient, *ht*	W/(m^2 °C)	1397	1436
annulus side film coefficient, *ha*	W/(m^2 °C)	9129	7449
overall heat transfer coefficient, *U*	W/(m^2 °C)	601.3	579.1
correction factor, *F*		0.979	1
tube side pressure drop, *dPt*	kPa	76.3	79.0
annulus side pressure drop, *dPa*	kPa	93.7	59.1

Table 10. Example 4 − Optimization Results

variable	unit	raw MINLP	linear-binary MINLP
tube side stream		cold stream	cold stream
total heat exchanger area, *A*	m^2	64.60	40.86
required heat exchanger area	m^2	55.92	37.01
inner tube NPS−OD	in−m	1 $^1/_4$ − 0.042	3 $^1/_2$ − 0.102
outer tube NPS−OD	in−m	2 $^1/_2$ − 0.073	4 $^1/_2$ − 0.127
hairpin length, *Lh*	ft−m	25−7.620	10−3.048
number of hairpins per unit, *Nh*		4	7
number of branches, *NB*		8	1
tube side units in parallel, *NPt*		1	1
annular side units in parallel, *NPa*		2	6
tube side velocity, *vt*	m/s	1.62	1.96
annulus side velocity, *va*	m/s	1.23	2.54
tube side film coefficient, *ht*	W/(m^2 °C)	420	656
annulus side film coefficient, *ha*	W/(m^2 °C)	1613	3276
overall heat transfer coefficient, *U*	W/(m^2 °C)	237.2	360.6
correction factor, *F*		0.992	0.986
tube side pressure drop, *dPt*	kPa	117.1	110.7
annulus side pressure drop, *dPa*	kPa	24.3	110.8

hairpins are built with a material with a thermal conductivity of 55 W/(m°C). The additional design specifications include flow velocity in both sides between 1 and 3 m/s for both examples, and a minimum excess area of 20% for example 3, and of 10% for example 4. The results obtained for example 3 and example 4, for both MINLP approaches, are depicted in Tables 9 and 10, and Figures 15 and 16, respectively. In the case of Table 9, there is a large difference between the number of branches associated with

DOI: 10.1021/acs.iecr.9b01536
Ind. Eng. Chem. Res. 2019, 58, 12080−12096

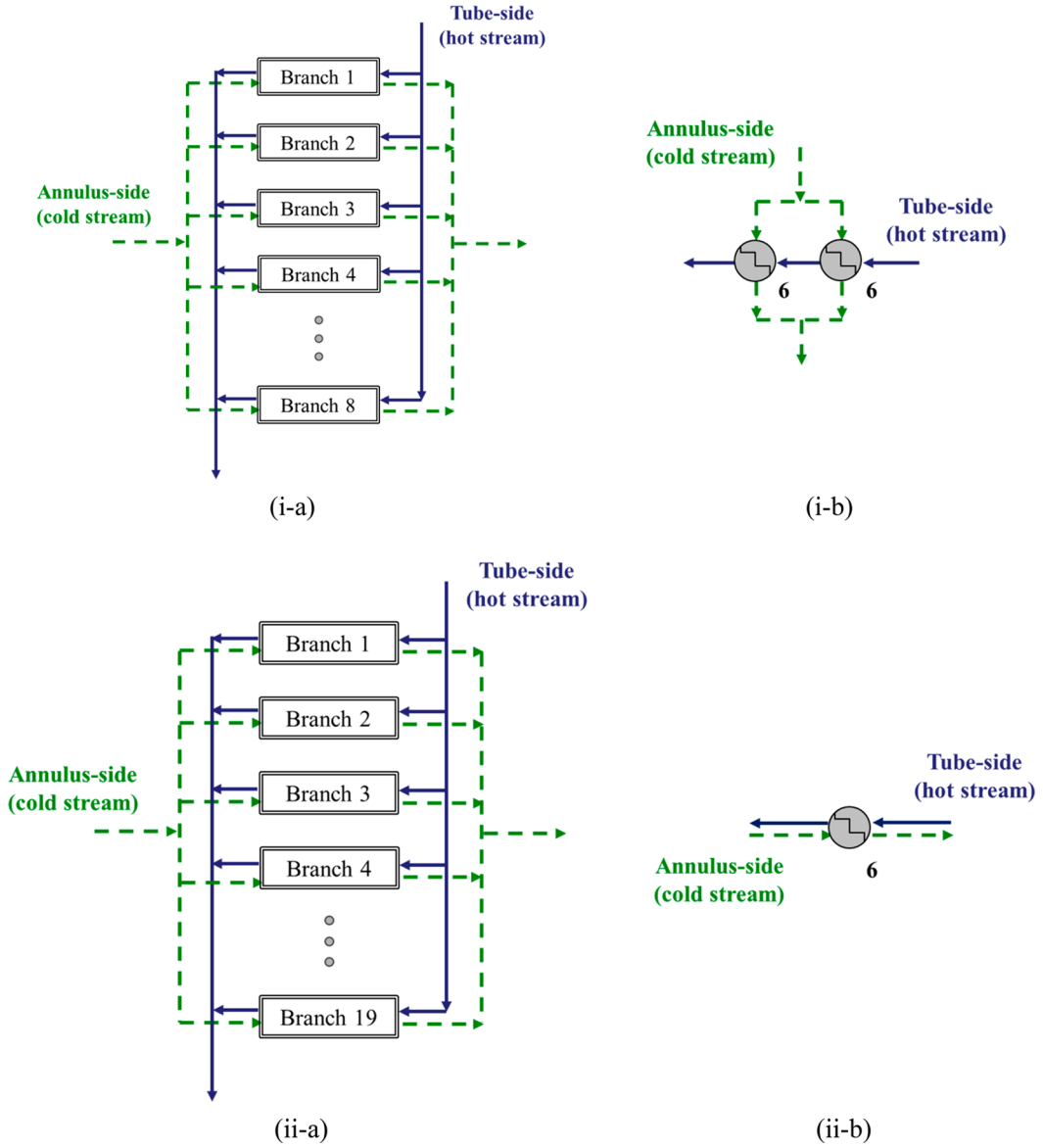

Figure 15. Example 3: (i) raw MINLP solutions; (ii) linear-binary. (a) General structure; (b) branch structure.

different structures, but there is a consistency between them. For the annular-flow side for example, in the solution obtained with the raw MINLP formulation there are eight branches (NB = 8), and in each branch there are two units in parallel (NPa = 2), while in the linear-binary MINLP solution, there are 19 branches (NB = 19) but there are no units in parallel in each branch (NPa = 1); therefore, in both cases the total flow for the annular side would be divided by 19. Since both inner and outer tubes had their OD's decreased from the first solution to the second, the annular flow area did not change significantly, and therefore, the velocities are quite similar in both cases (2 and 1.98 m/s). Now, if one looks to the tube flow side, there are 8 branches for the raw MINLP solution and 19 branches for the linear-binary solution, and in both cases there are no units in parallel (NPt = 1). Therefore, the mass flow per unit in the second case would be half the first one and a great decrease in the flow velocity would be expected. However, there is also a decrease in the available flow area per unit, since the inner tube OD goes from $1\,^{1}/_{2}$ in to 1 in., compensating a portion of the decrease in mass flow, so that the velocity only decreases from 1.71 to 1.41 m/s.

The computational times for both examples are shown in Table 11, indicating that the linear-binary MINLP approach requires more computational effort, which also occurred on the first two examples where the heat transfer areas obtained were the same for both formulations. These values were obtained using a computer with a processor Intel Core i7 3.41 GHz with 16.6 GB RAM memory.

To reformulate the problem to obtain the linear-binary MINLP, the problem variables and equations increase. This appears to be directly connected to the larger computational effort. For the given discrete available options given in examples 3 and 4, the raw MINLP has the number of 179 variables and 120 constraints, compared to 283 and 440 of the linear-binary approach.

The optimum values of the two MINLP approaches show that, for a given example, there may be more than one optimal solution. For example 3, the raw MINLP approach found a solution with a heat transfer area only 2.65% smaller than the one found with the linear-binary MINLP approach. On the contrary, for example 4 the smaller area was achieved using the

DOI: 10.1021/acs.iecr.9b01536
Ind. Eng. Chem. Res. 2019, 58, 12080−12096

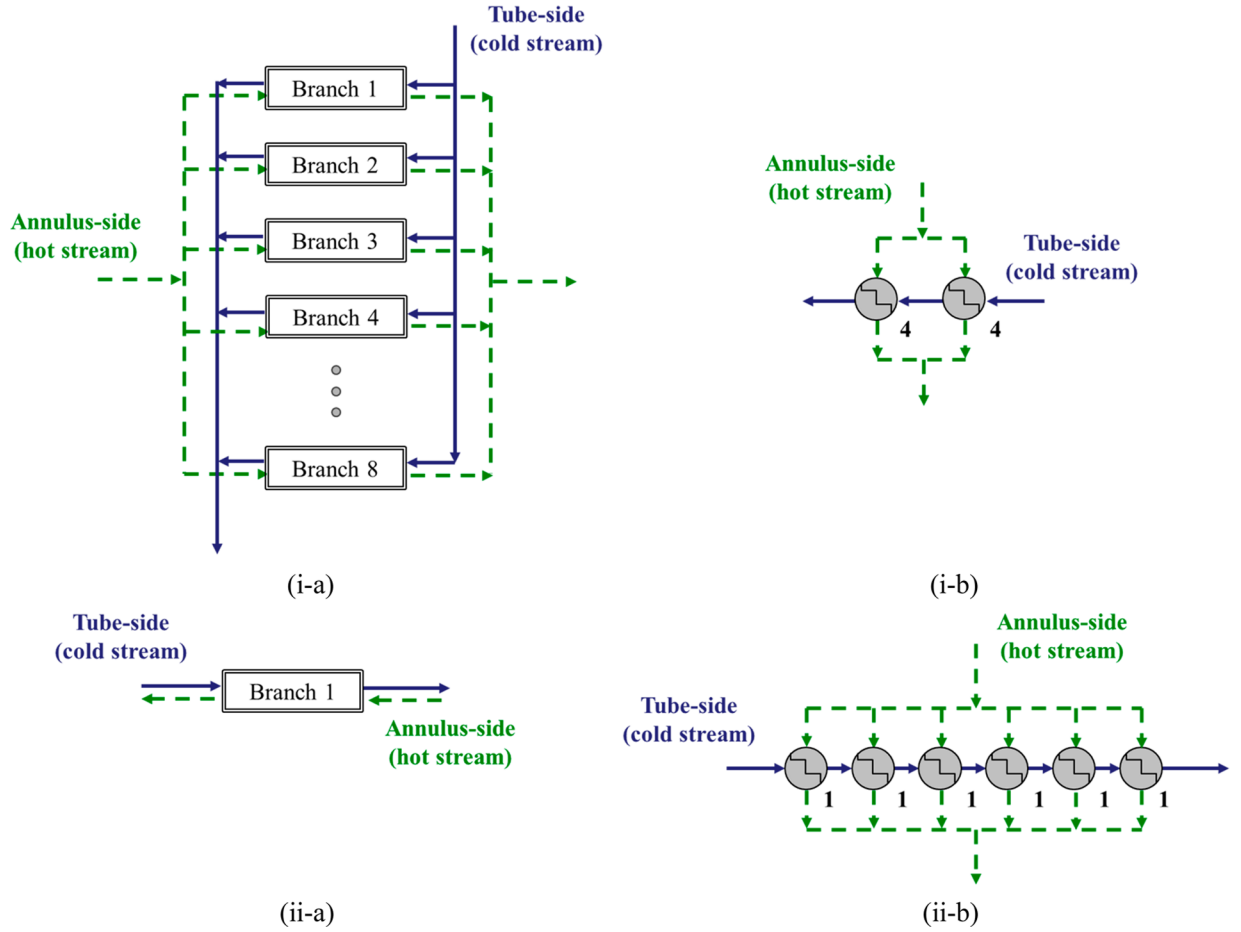

Figure 16. Example 4: (i) raw MINLP solutions; (ii) linear-binary. (a) General structure; (b) branch structure.

Table 11. Examples 3 and 4: Performance Comparison of the Two MINLP Approaches

	raw MINLP		linear-binary MINLP	
example	area (m^2)	elapsed time (s)	area (m^2)	elapsed time (s)
3	88.73	54.31	91.15	127.68
4	64.60	26.15	40.86	102.24

linear-binary MINLP approach, with a significant reduction of 36.7% when compared to the solution obtained with the raw MINLP result. The results do not show any pattern regarding which formulation is able to achieve a better solution, but the wide difference between solutions in example 4 illustrates the importance of the utilization of a global optimization scheme to address the design problem.

Thus, both MINLP approaches were also solved with BARON considering (i) no initial estimates, (ii) the same initial estimates used to run the problem using the solver SBB, and (iii) initial estimates obtained from the solution of the SBB. The results are shown in Table 12.

For all three scenarios the global optimal solution was achieved for both examples 3 and 4. There was no significant computational effort gained between scenarios (i) and (ii). In scenario (iii), in which the solutions obtained from sBB runs were employed as initial estimates, there is a significant reduction in computational effort for the BARON run isolated. Since it is necessary to generate the initial estimates first by a sBB optimization run, the computational effort shown in Table 12 corresponds to the sum of both elapsed times. Nevertheless, in two situations (example 3 with linear-binary approach and example 4 solved with raw MINLP approach), the gains are approximately 28% and 89%, respectively, showing that the methodology proposed here can also be applied as a preprocessing method for global optimization procedures.

Table 12. Elapsed Time Comparison of BARON Solver with Different Initial Estimates

		Elapsed time (s)					
		(i) GAMS default initial estimates		(ii) same initial estimates as the ones used for sBB solver		(iii) results from sBB solver used as initial estimates	
example	area (m^2)	raw MINLP	linear-binary MINLP	raw MINLP	linear-binary MINLP	raw MINLP	linear-binary MINLP
3	88.73	279.04	407.82	279.90	407.77	269.91	294.14
4	40.86	796.15	400.26	718.52	390.02	84.39	386.51

DOI: 10.1021/acs.iecr.9b01536
Ind. Eng. Chem. Res. 2019, 58, 12080−12096

7. CONCLUSIONS

This paper presented the solution of the design problem of double pipe heat exchangers using mathematical programming. The design variables are selected among discrete values, due to their physical nature or available commercial alternatives. Therefore, the problem is formulated as an MINLP problem, which is presented here in two versions. The first approach (raw MINLP) is based on the original nonlinear equations and the second approach (linear-binary MINLP) involves mathematical transformations that eliminate the nonlinearities in the binary variables, rendering a linear model in those. A comparison with the literature shows that our MINLP approach can obtain a solution superior to that of trial and verification. The application of the original and modified formulations to a sample of design problems indicated that the latter approach demands more computational time. The analysis of the heat transfer area of the solutions indicated the presence of multiple locally optimal solutions. The large difference between the objective functions in a pair of local optima, resultant of the nonconvexity of the MINLP, illustrates the importance of the investigation of alternatives that can identify rigorously the global optimum.

■ ASSOCIATED CONTENT

Supporting Information

The Supporting Information is available free of charge on the ACS Publications website at DOI: 10.1021/acs.iecr.9b01536.

Equations resultant from the MINLP reformulation (linear-binary MINLP); formulation using Serth's correlations employed in example 1; steps of the heuristic procedure applied to example 2; additional examples that explore the flexibility of the proposed model (PDF)

■ AUTHOR INFORMATION

Corresponding Author

*E-mail: andrehc@uerj.br.

ORCID

André L. H. Costa: 0000-0001-9167-8754

Miguel J. Bagajewicz: 0000-0003-2195-0833

Notes

The authors declare no competing financial interest.

■ ACKNOWLEDGMENTS

Julia C. Lemos thanks the Coordination for the Improvement of Higher Education Personnel (CAPES) for the postdoctoral fellowship through the PNPD Program. André L. H. Costa thanks Rio de Janeiro State University (UERJ) for the financial support through the Prociência Program and the National Council for Scientific and Technological Development (CNPq) for the research productivity fellowship (Process 311225/2016-0).

■ NOMENCLATURE

Parameters

$\widehat{\Delta P}_{sSTdisp}$ = Stream *sST* available pressure drop (Pa)

$\widehat{\Delta Tlm}$ = Logarithmic mean temperature (°C)

$\hat{\mu}_{sST}$ = Stream *sST* viscosity (Pa·s)

$\hat{\rho}_{sST}$ = Stream *sST* density (kg/m^3)

$\hat{\Phi}$ = Nonlinear continuous functions upper limit

$\hat{A}_{exc}$ = Minimum area excess (%)

$\widehat{Cp}_{sST}$ = Stream *sST* heat capacity (J/(kg °C))

$\hat{k}_{sST}$ = Stream *sST* thermal conductivity (W/(m °C))

$\widehat{ktube}$ = Tube material's thermal conductivity (W/m °C)

$\hat{m}_{sST}$ = Stream *sST* mass flow (kg/s)

$\widehat{pdte}_{sd}$ = Available inside tube external diameters (m)

$\widehat{pDte}_{sD}$ = Available outside tube external diameters (m)

$\widehat{pdti}_{sd}$ = Available inside tube internal diameters (m)

$\widehat{pDti}_{sD}$ = Available outside tube internal diameters (m)

$\widehat{pF}_{sST,sE}$ = F factor in case stream *sST* is in series, for $sE \neq 1$

$\widehat{ph}$ = Objective function penalty factor

$\widehat{pP}_{sST}$ = P parameter for the calculation of F factor if the stream *sST* is in series

$\widehat{pR}_{sST}$ = R parameter for the calculation of F factor if the stream *sST* is in series

$\widehat{pLh}_{sLh}$ = Available hairpin lengths (m)

$\widehat{pNB}_{sB}$ = Number of available branches

$\widehat{pNE}_{sE}$ = Number of available heat exchangers in series by branch

$\widehat{pNh}_{sNh}$ = Number of available hairpins per unit

$\hat{Q}$ = Heat-transfer rate (W)

$\widehat{Rf}_{sST}$ = Stream *sST* fouling resistance (m^2 °C/W)

$\widehat{Ti}_{sST}$ = Stream *sST* inlet temperature (°C)

$\widehat{To}_{sST}$ = Stream *sST* outlet temperature (°C)

$\widehat{UNu}$ = Nusselt number upper limit

$\widehat{UPr}$ = Prandtl number upper limit

$\widehat{URe}$ = Reynolds number upper limit

$\widehat{va}_{max}$ = Annulus-side maximum velocity (m/s)

$\widehat{va}_{min}$ = Annulus-side minimum velocity (m/s)

$\widehat{vt}_{max}$ = Tube-side maximum velocity (m/s)

$\widehat{vt}_{min}$ = Tube-side minimum velocity (m/s)

Continuous variables

ΔPa = Annulus-side pressure drop (Pa)

ΔPt = Tube-side pressure drop (Pa)

μa = Annulus-side stream viscosity (Pa·s)

μt = Tube-side stream viscosity (Pa·s)

ρa = Annulus-side stream density (kg/m^3)

ρt = Tube-side stream density (kg/m^3)

A = Heat transfer area (m^2)

A_{req} = Required heat transfer area (m^2)

Aa = Annulus-side flow area (m^2)

At = Tube-side flow area (m^2)

Cpa = Annulus-side stream heat capacity (J/(kg °C))

Cpt = Tube-side stream heat capacity (J/(kg °C))

dh = Hydraulic diameter (m)

dte = Inner tube external diameter (m)

Dte = Outside tube external diameter (m)

dti = Inner tube internal diameter (m)

Dti = Outside tube internal diameter (m)

F = Correction factor

fa = Annulus-side friction factor

fa^{lam} = Annulus-side friction factor for laminar flow

fa^{tran} = Annulus-side friction factor for transitional flow

fa^{turb} = Annulus-side friction factor for turbulent flow

ft = Tube-side friction factor

ft^{lam} = Tube-side friction factor for laminar flow

ft^{tran} = Tube-side friction factor for transitional flow

DOI: 10.1021/acs.iecr.9b01536
Ind. Eng. Chem. Res. 2019, 58, 12080−12096

ft^{turb} = Tube-side friction factor for turbulent flow
ha = Annulus-side convective heat transfer coefficient (W/(m^2 °C))
ht = Tube-side convective heat transfer coefficient (W/(m^2 °C))
ka = Annulus-side stream thermal conductivity (W/(m °C))
kt = Tube-side stream thermal conductivity (W/(m °C))
La = Annulus-side hydraulic length (m)
Lh = Length of a hairpin (m)
Lt = Tube-side hydraulic length (m)
Lu = Length of a unit (m)
ma = Annular region mass flow (kg/s)
mt = Inside tube mass flow (kg/s)
NB = Number of parallel branches
Nh = Number of hairpins per unit
NPa = Annulus-side units in parallel per branch
NPt = Tube-side units in parallel per branch
Nua = Annulus-side Nusselt number
Nua^{Gni} = Annulus-side Gnielinski Nusselt number
Nua^{Hau} = Annulus-side Hausen Nusselt number
$Nua^{S\&T}$ = Annulus-side Seider and Tate Nusselt number
Nua^{theo} = Annulus-side theoretical Nusselt number
Nut = Tube-side Nusselt number
Nut^{Gni} = Tube-side Gnielinski Nusselt number
Nut^{Hau} = Tube-side Hausen Nusselt number
$Nut^{S\&T}$ = Tube-side Seider and Tate Nusselt number
Nut^{theo} = Tube-side theoretical Nusselt number
Pra = Annulus-side stream Prandtl number
Prt = Tube-side stream Prandtl number
Rea = Annulus-side stream Reynolds number
Ret = Tube-side stream Reynolds number
Rfa = Annulus-side stream fouling resistance (m^2 °C/W)
Rft = Tube-side stream fouling resistance (m^2 °C/W)
U = Overall heat transfer coefficient (W/(m^2 °C))
va = Annulus-side velocity (m/s)
vt = Tube-side velocity (m/s)

Binary variables

yB_{sB} = Number of branches selection
yd_{sd} = Inner tube diameter selection
yD_{sD} = Outer tube diameter selection
yLh_{sLh} = Hairpin tube length selection
yNh_{sNh} = Number of hairpins per unit selection
$yNua_{sNua}$ = Range of annular region Seider and Tate Nusselt number selection
$yNut_{sNut}$ = Range of inner tube Seider and Tate Nusselt number selection
yPa_{sE} = Annulus-side number of units in parallel per branch selection
$yPra_{sPra}$ = Range of annular region Prandtl number selection
$yPrt_{sPrt}$ = Range of inner tube Prandtl number selection
yPt_{sE} = Tube-side number of units in parallel per branch selection
$yRea_{sRea}$ = Range of annular region Reynolds number selection
$yRet_{sRet}$ = Range of inner tube Reynolds number selection
yT_{sST} = Stream sST allocation (1 = tube-side; 0 = annulus-side)

Subscripts

sB = Index of number of branches
sd = Index of inner tube diameters
sD = Index of outer tube diameters
sE = Index of number of units per branch
sL = Index of tube length
$sNua$ = Index of ranges of annular region Seider and Tate Nusselt number
$sNut$ = Index of ranges of inner tube Seider and Tate Nusselt number
$sPra$ = Index of ranges of annular region Prandtl number
$sPrt$ = Index of ranges of inner tube Prandtl number
$sRea$ = Index of ranges of annular region Reynolds number
$sRet$ = Index of ranges of inner tube Reynolds number
sST = Index of streams

REFERENCES

(1) Towler, G.; Sinnott, R. *Chemical Engineering Design Principles, Practice and Economics of Plant and Process Design*; Butterworth-Heinemann: Burlington, 2008.
(2) Kakaç, S.; Liu, H. *Heat Exchangers Selection, Rating and Thermal Design*; CRC Press: Boca Raton, 2002.
(3) Guy, A. R. Operational advantages. *Heat Exchanger Design Handbook*; Hewitt, G. F., Ed.; Begell House: New York, 2008.
(4) Omidi, M.; Farhadi, M.; Jafari, M. A comprehensive review on double pipe heat exchangers. *Appl. Therm. Eng.* **2017**, *110*, 1075.
(5) Sahiti, N.; Krasniqi, F.; Fejzullahu, X.; Bunjaku, J.; Muriqi, A. Entropy generation minimization of a double-pipe pin fin heat exchanger. *Appl. Therm. Eng.* **2008**, *28*, 2337.
(6) Syed, K. S.; Iqbal, Z.; Ishaq, M. Optimal configuration of finned annulus in a double pipe with fully developed laminar flow. *Appl. Therm. Eng.* **2011**, *31*, 1435.
(7) Iqbal, Z.; Syed, K. S.; Ishaq, M. Optimal convective heat transfer in double pipe with parabolic fins. *Int. J. Heat Mass Transfer* **2011**, *54*, 5415.
(8) Iqbal, Z.; Syed, K. S.; Ishaq, M. Optimal fin shape in finned double pipe with fully developed laminar flow. *Appl. Therm. Eng.* **2008**, *51*, 1202.
(9) Han, H.; Bing-Xi, L.; Wu, H.; Shao, W. Multi-objective shape optimization of double pipe heat exchanger with inner corrugated tube using RSM method. *Int. J. Therm. Sci.* **2015**, *90*, 173.
(10) Dastmalchi, M.; Sheikhzadeh, G. A.; Arefmanesh, A. Optimization of micro-finned tubes in double pipe heat exchangers using particle swarm algorithm. *Appl. Therm. Eng.* **2017**, *119*, 1.
(11) Söylemez, M. S. Thermoeconomical Optimization of Double-Pipe Heat Exchanger for Waste heat Recovery. *J. Thermophys. Heat Transfer* **2004**, *18*, 559.
(12) Swamee, P. K.; Aggarwal, N.; Aggarwal, V. Optimum design of double pipe heat exchanger. *Int. J. Heat Mass Transfer* **2008**, *51*, 2260.
(13) Serth, R. W. *Process Heat Transfer Principles and Applications*; Academic Press: Burlington, 2007.
(14) Duran, M. A.; Grossmann, I. E. An outer-approximation algorithm for a class of mixed-integer nonlinear programs. *Mathematical Programming* **1986**, *36*, 307.
(15) Saunders, E. A. D. *Heat Exchangers Selection, Design and Construction*; John Wiley & Sons: New York, 1988.
(16) Incropera, F. P.; Dewitt, D. P. *Fundamentals of Heat and Mass Transfer*; John Wiley & Sons: New York, 2007.
(17) Williams, H. P. *Model Building in Mathematical Programming*; Wiley: New York, 2013.

DOI: 10.1021/acs.iecr.9b01536
Ind. Eng. Chem. Res. 2019, 58, 12080−12096